Tropical Drivers of Interannual Vegetation Variability in Eastern Africa

In-Won Kim (iwkimi@pusan.ac.kr)
Center for Climate Physics, Institute for Basic Science
Malte Stuecker
University of Hawai'i Sea Grant
Axel Timmermann
Center for Climate Physics, Institute for Basic Science
Jong-Seong Kug
Pohang University of Science and Technology
So-Won Park
Pohang University of Science and Technology
Jin-Soo Kim
University of Zurich

Research Article

Keywords: tropical Pacific, sea surface temperature (SST), Tropical Indian Ocean (TIO), Indian Ocean warming

Posted Date: January 19th, 2021

DOI: https://doi.org/10.21203/rs.3.rs-144842/v1

Tropical drivers of interannual vegetation variability in eastern Africa

In-Won Kim[1,2]*, Malte F. Stuecker[3], Axel Timmermann[1,2], Jong-Seong Kug[4], So-Won Park[4], and Jin-Soo Kim[5]

[1] Center for Climate Physics, Institute for Basic Science, Busan, Republic of Korea
[2] Pusan National University, Busan, Republic of Korea
[3] Department of Oceanography and International Pacific Research Center, School of Ocean and Earth Science and Technology, University of Hawai'i at Mānoa, Honolulu, HI, USA
[4] Division of Environmental Science and Engineering, Pohang University of Science and Technology, Pohang, Republic of Korea
[5] Department of Evolutionary Biology and Environmental Studies, University of Zurich, Zurich, Switzerland

*Corresponding author: In-Won Kim (iwkimi@pusan.ac.kr)

ABSTRACT

Mechanisms by which tropical Pacific and Indian Ocean sea surface temperatures influence vegetation in Eastern Africa and which role drought-induced fires play have not been fully explored. Here, we use a suite of idealized Earth system model simulations to elucidate the governing processes for eastern African interannual vegetation changes. Our analysis focuses on Tanzania. In the absence of ENSO-induced sea surface temperature (SST) anomalies in the Tropical Indian Ocean (TIO), El Niño causes during its peak phase negative precipitation anomalies over Tanzania due to a weakening of the tropical-wide Walker circulation and anomalous descending motion over the Indian Ocean and southeastern Africa. Resulting drought conditions increase the occurrence of wildfires, which leads to a marked decrease in vegetation cover. Subsequent wetter La Niña conditions in boreal winter reverse the trend in vegetation, causing a gradual 1-year-long recovery phase. The 2-year-long vegetation response in Tanzania can be explained as a double-integration of the local rainfall anomalies, which originate from the seasonally-modulated ENSO Pacific-SST forcing (Combination mode). In the presence of interannual TIO SST forcing, the southeast African precipitation and vegetation responses to ENSO are muted due to Indian Ocean warming and the resulting anomalous upward motion in the atmosphere.

Introduction

Natural fluctuations in Africa's vegetation are affected by rainfall and wildfire variability[1-7]. Especially the Sahel, eastern Africa, and southern Africa show large interannual variations in terrestrial productivity, which can be attributed to year-to-year changes in water stress[8].

The El Niño-Southern Oscillation (ENSO) has been considered a primary climate driver for rainfall variability in parts of Africa. Evidence from observations shows that El Niño events can cause drought in southern Africa, and enhanced precipitation and corresponding floods in eastern Africa[9]. Earlier studies documented a strong relationship between ENSO and the Normalized Difference Vegetation Index (NDVI) over eastern and southern Africa[10-13]. In contrast, over the Sahel, the relationship between ENSO and NDVI is weak[14].

Observations and model experiments show an asymmetric atmospheric response over Africa between El Niño and La Niña[15]. In addition, nonlinear ENSO teleconnections over Africa might be also affected by ENSO-induced asymmetric sea surface temperature (SST) responses over the Atlantic and Indian Oceans. SST variability over the south Atlantic Ocean influences rainfall over the Sahel in the opposite sense of ENSO[10]. Indian Ocean Dipole (IOD) events, typically accompanied by ENSO, positively correlate with eastern African rainfall during the short rainy season[16,17]. Apart from ENSO, the vegetation response to climate factors is also modulated by nonlinear land processes. Globally, a nonlinear relationship between net primary production and rainfall is observed for grasslands[18]. Interannual vegetation changes over eastern Africa show a nonlinear relationship with rainfall variability and a strong dependency on land cover type is observed[2].

Although the aforementioned studies have demonstrated the impacts of ENSO on African vegetation based on observations, we still lack a deeper understanding of how interannual SST changes in the Indian and Pacific Ocean influence vegetation anomalies and which role wildfires play. In this study, we investigate the vegetation response over sub-Saharan Africa to ENSO through a series of model experiments and compare them to the observations.

Results

The Walker circulation response to ENSO

To investigate the drivers of the vegetation response over Africa, we first focus on the tropical large-scale atmospheric circulation and its interannual variations. The position and strength of the Walker circulation are closely coupled to SST anomalies in the tropical Pacific. Both the Periodic and the Pacific experiments (SST anomalies are only prescribed in the tropical Pacific) show pronounced Walker circulation changes between El Niño and La Niña events with anomalous ascending motion over the eastern Pacific region (and corresponding upper-level divergence) and anomalous descending motion (and corresponding upper-level convergence) during the peak ENSO phase of December-January-February [D(0)JF(1)] (Fig. 1a, b). Importantly, the edge of the descending motion extends to the African continent in the two experiments. In contrast, the Tropics experiment shows that the center of the descending motion shifts toward the Maritime Continent, inducing weaker subsidence around the Indian and Atlantic Ocean, accompanying tropical Indian Ocean (TIO) warming (Fig. 1c). This large-scale circulation response is similar to what is seen for the observations (Fig. 1d). The TIO warming pattern seen in Figure 1c, d is largely forced by El Niño and then is prolonged for several months after the El Niño event due to the so-called capacitor effect[19,20]. The pattern of

large-scale atmospheric anomalies in the Tropics experiment (Fig. 1c) is more consistent with the observations (Fig. 1d) than the Periodic and Pacific experiments (Fig. 1a, b). This suggests that TIO warming affects the change of the large-scale atmospheric circulation around the African continent related to ENSO, as suggested by Liu *et al.*[21].

The response of rainfall, vegetation, and wildfire over Africa to ENSO

Here, to focus on the symmetric (i.e., linear) response to El Niño and La Niña events, we show El Niño minus La Niña composites. Observed composite differences between El Niño and La Niña events display pronounced positive precipitation anomalies over the Horn of Africa and negative anomalies over Southern Africa in D(0)JF(1) (Fig. 2j). The three experiments (Periodic, Pacific, and Tropics) reproduce these anomalies reasonably well (Fig. 2a, d, g). However, a small positive precipitation anomaly simulated by the Tropics experiment in the northeastern part of South Africa is not captured in the observations.

Interestingly, the Periodic and the Pacific experiments exhibit a 50 % D(0)JF(1) rainfall reduction over Tanzania for the El Niño minus La Niña composite (Fig. 2a, d) and an accompanying negative Net Primary Production (NPP) anomaly during January-February-March of the decaying ENSO year [JFM(1)] (Fig. 2b, e). In contrast, the observations and the more realistic Tropics experiment show only very weak rainfall, NPP, and LAI anomalies over Tanzania (Fig. 2g, 2h, 2i, 2j, 2l), in agreement with Latif *et al.*[22]. This suggests that tropical Indian or Atlantic Ocean SST anomalies might play an important role in muting the direct Pacific response over this region. We hypothesize specifically that the negligible observed rainfall response over Tanzania in the observations can be attributed to a compensation between the direct Pacific effect and the El Niño-related Indian Ocean warming effect on the Walker circulation (Fig. 1b, c).

This hypothesis is further supported by the lead-lag relationship between ENSO and LAI anomalies in the Periodic and the Pacific experiments (Fig. 2k). According to this analysis ENSO is leading LAI anomalies in Tanzania by about one year in these two experiments, whereas no statistically significant correlation can be found in the Tropics experiment. ENSO negatively correlates with LAI over Tanzania at a maximum lag of 16-months (R = 0.49, $p < 0.00001$) in the Pacific and 18-months (R = 0.58, $p < 0.00001$) in the Periodic experiments (Fig. 2k). In contrast, for the Tropics experiment, the correlation is not significant (R = 0.06, p=0.11) (Fig. 2k). Regarding the LAI response to ENSO at this 16-18 months lag (that is, in May-June-July in year 2 after the ENSO event peak time: MJJ(2)), we find larger negative anomalies over Tanzania in the Pacific and the Periodic experiments (Fig. 2c, f), while they are much weaker anomalies in the Tropics experiment and the observations (Fig. 2i, l). Moreover, the delayed response over Tanzania to ENSO is also found in wildfire activity (Fig. 3). The periodic experiment shows negative anomalies in burned area over Tanzania in D(0)JF(1) and statistically insignificant differences in the Pacific and Tropics experiments, as well as in the observations. However, the Periodic and the Pacific experiments show a 10-20 % increase in burned area over Tanzania in September-October-November in year 1 after ENSO event peak time [SON(1)] (Fig. 3a-d), whereas the observations and the Tropics experiment show statistically insignificant differences (Fig. 3e-h).

Combination mode-driven rainfall response over Tanzania

The temporal evolution of the rainfall response over Tanzania to ENSO shows a rapid transition during the peak phase of both El Niño and La Niña in both the Periodic and the Pacific experiments, but not in the Tropics experiment (Fig. 4). The rainfall response is particularly pronounced in the former during the peak phase of ENSO in D(0)JF(1), which is also the climatological wet season (Fig. 4, Fig. S2). This illustrates the tight coupling between climatological conditions and the imposed ENSO signal. To further understand the distinct atmospheric response to ENSO in the absence of TIO SST anomalies, we hypothesize that the precipitation response over Tanzania to ENSO is driven by the seasonally modulated interannual ENSO variability, which is referred to as a Combination mode (C-mode)[23]. According to this simple model the precipitation anomalies can be written as

$$\boldsymbol{P^*(t) = \alpha\ ENSO\ (t) + \ \beta\ ENSO(t) \cdot \cos(\omega_a t)\ (1)},$$

where α and β are the regression coefficients on the ENSO and theoretical C-mode predictors, and ω_a the frequency of the annual cycle. One can also include a white noise precipitation forcing, but since we consider ensemble mean properties in a linear model, the noise forcing is not necessary to understand the temporal evolution. The time-series in the Periodic and Pacific experiments show that the reconstructions of precipitation anomalies over Tanzania via the C-mode equation reproduce the seasonally varying simulated rainfall response to ENSO well (Periodic: R=0.64, $p < 0.00001$; Pacific: R= 0.65, $p < 0.00001$) (Fig. 4). The simulated La Niña response is somewhat reduced as compared to the El Niño rainfall anomaly. This is reminiscent of an atmospheric nonlinearity to otherwise symmetric SST forcing.

Role of wildfires in the vegetation response to ENSO

Wildfires can play a potential role in vegetation change through climate-fire-vegetation interactions[24,25]. In the absence of TIO warming in the Periodic and Pacific experiments, El Niño induced drying increases the occurrence of fires, which is manifest in the prolonged positive anomalies in burned area lasting for about one year after the peak of El Niño (Fig. 4 a, b). For wet savannas in Africa, an increase in fuel moisture can lead to a decrease in the burned area[7], while for dry savannas, an increase in moisture facilitates more fires[26]. To investigate the causal linkages between precipitation and wildfire responses to ENSO, we hypothesize that changes in burned area B, are driven by precipitation variability P^*. Here we choose P^* as the ENSO-reconstructed precipitation anomaly from equation (1). We assume in its simplest linearized form that the burned area does not depend on the available vegetation which allows us to introduce a fixed mean recovery timescale (μ^{-1}), in which the burned area can regrow. The simplified linearized model then reads:

$$\boldsymbol{\frac{dB(t)}{dt} = -\mu_1 B - \theta_1 P^*(t)(2)}.$$

Appropriate parameters values are given in Table S1. The reconstruction of burned area response over Tanzania captures the simulated temporal evolution reasonably well (R=0.82, $p < 0.00001$), suggesting that the burned area response can be determined essentially by the time integral of the direct ENSO effect and the C-mode term. Previous studies support the notion that the lagged response of wildfire activity in some areas can be linked to the integrated effect of antecedent precipitation anomalies[7,27]. In the Periodic experiment, less rainfall over Tanzania during the wet season [D(0)JF(1)] and successive dry season promote a lagged response in burned area in SON(1) (Fig. S2). Subsequently, LAI anomalies over Tanzania slowly develop after the peak of El Niño and are prolonged until the following La Niña event. Especially, the peak of negative anomalies in

LAI occurs during the mature La Niña phase in December-January-February in year 2 [DJF(2)], in spite of the maximum rainfall anomalies during this time (Fig. 4, Fig. S2). The vegetation response to climate factors also depends on vegetation resistance and resilience[28]. Accordingly, we hypothesize that the LAI response can be largely explained by the integrated effect of burned area (equation 2), where L represents temporal variation of LAI, and λ is 8 month^{-1} as an inverse damping time scale (characterizing vegetation resilience):

$$\frac{dL(t)}{dt} = -\ \mu_2 L - \theta_2 B(t) \quad (3).$$

According to this simplified double-integration model (equations 1-3) the LAI response over Tanzania correlates highly with simulated LAI anomalies (R=0.72, $p < 0.00001$), indicating that the lagged and prolonged vegetation response to ENSO is explained by vegetation resilience and the integrated effect of wildfire activity. Similar double-integration models have been introduced to explain also the emergence of low-frequency marine biogeochemical variability[29].

Discussion and Conclusions

In this study, we explored how vegetation in the southeastern part of Africa changes in response to interannual ENSO variability through a series of model experiments. Focusing on Tanzania, we found that, in the absence of TIO variability, the rapid transition of precipitation anomalies during ENSO events are determined by the interaction between ENSO and the annual cycle (the so-called C-mode). After the occurrence of El Niño, the pronounced decrease in rainfall over Tanzania leads to enhancement in burned area with a time delay, thereby prolonging a marked vegetation decrease for 2 years. This response can be explained by the integrated effect of wildfire (double integrated effect of precipitation) and vegetation resilience through an idealized dynamical model, which explains the AGCM results reasonably well.

However, in the real world, there is no evidence for robust changes in precipitation, wildfire, and vegetation over Tanzania, in relationship to ENSO. This is because TIO warming during El Niño events compensates the rainfall response to ENSO over Tanzania (Fig. 4c) by weakening the anomalous atmospheric subsidence (Fig. 1b, c). This offset response is consistent with the opposite impact between Indian Ocean Basin-wide mode (IOBM) and ENSO on seasonal rainfall variability over Africa discussed in Preethi *et al.*[30]. The IOD is another primary climate factor which can affect rainfall and vegetation variability over East Africa[2,30,31], but the IOD impact to eastern Africa peaks in September-November [SON(0)] (Fig. S3). This is too early to cause major precipitation and vegetation anomalies in Tanzania (Fig. 4, Fig. S3).

Furthermore, we emphasize the necessity to understand African vegetation variations driven by the interaction between ENSO and TIO warming under a warmer climate through further studies. Future projections show that TIO warming related to ENSO will likely be intensified[32-34]. Thus, our results provide a framework to assess future coupled changes in rainfall, wildfires, and vegetation induced by the relationship between ENSO and TIO warming in response to global warming.

Data and Experiments

Observations

We used precipitation data from Global Precipitation Analysis Products of the Global Precipitation Climatology Centre (GPCC)[35], 200 hPa wind from European Centre for Medium-Range Weather Forecasts

(ECMWF) reanalysis generation 5 (ERA5)[36], and SST from the Hadley Centre Sea Ice and Sea Surface Temperature data set version 1 (HadISST1)[37]. To characterize observed vegetation changes, we utilized leaf area index (LAI) data derived from the Global Inventory Modeling and Mapping Studies (GIMMS) Normalized Difference Vegetation Index (NDVI3g) for the period 1982 to 2011[38]. The monthly Global Fire Emissions Database version 4 (GFEDv4)[39] was used to characterize the 1994-2014 wildfire activity.

Model and Experiments

We conducted a suite of atmospheric general circulation model (AGCM) experiments with the Community Earth System Model (CESM 1.2.2) using the Community Atmosphere Model version 4.0 (CAM4)[40] and Community Land Model version 4.0 (CLM4)[41,42] with active Carbon-Nitrogen (CN) biogeochemistry. The model, which uses a horizontal of approximately 1-degree, was spun up until the carbon and nitrogen pools were equilibrated to a 1957-2016 SST climatology boundary forcing and present-day greenhouse gas concentrations. We then performed four different types of AGCM experiment ensembles to investigate the vegetation response over sub-Saharan Africa to interannual tropical SST variability starting from these equilibrated initial conditions.

First, a control experiment (CTRL) was carried out with a repeating global climatological SST forcing for the period 1957-2016 using a 3-member ensemble. The CTRL largely reproduces the observed precipitation (PRCP), LAI, and burned area climatological patterns. Climatological mean precipitation over central Africa and southeastern Africa and burned area over some parts of Ethiopia, Tanzania, Angola, and South Africa are somewhat overestimated in the model (Figure S1).

To illustrate the impact of observed ENSO variability, a "Pacific" experiment was conducted by adding the observed SST anomalies over the tropical eastern Pacific (15°S-15°N, 180°-90°W) for the period 1957-2016 to the climatology with a 10-member ensemble. A "Tropics" experiment was forced with SST anomalies over the whole tropics (15°S-15°N) for the period 1957-2016 to investigate the response to other modes of pantropical SST variability in addition to ENSO with a 3-member ensemble. An idealized "Periodic" experiment was designed to investigate the response to symmetric ENSO variability (see for instance Stuecker *et al.*[43]). The regressed ENSO SST anomaly pattern over the tropical eastern Pacific with an idealized sinusoidal 2.5 years periodicity was added to the observed SST climatology (1957-2016) and the experiment was run for 100 years with a 3-member ensemble. The climate response in all perturbation experiments is defined relative to the control experiment climate. Outside the tropical SST perturbation regions, the SST is the same as in the CTRL simulation.

Acknowledgments

I.-W. Kim and A. Timmermann were supported by the Institute for Basic Science (project code IBS-R028-D1). I.-W. Kim thanks K. Rodgers for comments and editing of the manuscript. M. F. Stuecker thanks Abigail Swann, Marysa Laguë, and Keith Oleson for discussions on CLM. J.-S. Kug and S.-W. Park were supported by NRF-2018R1A5A1024958. J.-S. Kim was supported by University of Zurich Research Priority Programme "Global Change and Biodiversity" (URPP GCB). This is SOEST publication X and IPRC contribution Y.

Author contributions

I.-W.K. performed the analysis and wrote the initial draft of the manuscript. A.T. and M.F.S. designed the study. M.F.S. conducted the idealized model experiments. All authors discussed the results and reviewed the manuscript.

References

1 Camberlin, P., Martiny, N., Philippon, N. & Richard, Y. Determinants of the interannual relationships between remote sensed photosynthetic activity and rainfall in tropical Africa. *Remote Sensing of Environment* **106**, 199-216 (2007).

2 Hawinkel, P. *et al.* Vegetation response to precipitation variability in East Africa controlled by biogeographical factors. *Journal of Geophysical Research: Biogeosciences* **121**, 2422-2444 (2016).

3 Musau, J., Patil, S., Sheffield, J. & Marshall, M. Spatio-temporal vegetation dynamics and relationshipwithclimate over East Africa. (2016).

4 Archibald, S., Nickless, A., Govender, N., Scholes, R. J. & Lehsten, V. Climate and the inter-annual variability of fire in southern Africa: a meta-analysis using long-term field data and satellite-derived burnt area data. *Global Ecology and Biogeography* **19**, 794-809 (2010).

5 Andela, N. & Van Der Werf, G. R. Recent trends in African fires driven by cropland expansion and El Nino to La Nina transition. *Nature Climate Change* **4**, 791-795 (2014).

6 Papagiannopoulou, C. *et al.* Vegetation anomalies caused by antecedent precipitation in most of the world. *Environmental Research Letters* **12**, 074016 (2017).

7 Zubkova, M., Boschetti, L., Abatzoglou, J. T. & Giglio, L. Changes in fire activity in Africa from 2002 to 2016 and their potential drivers. *Geophysical research letters* **46**, 7643-7653 (2019).

8 Williams, C. A. *et al.* Interannual variability of photosynthesis across Africa and its attribution. *Journal of Geophysical Research: Biogeosciences* **113** (2008).

9 Nicholson, S. E. & Kim, J. The relationship of the El Niño–Southern oscillation to African rainfall. *International Journal of Climatology: A Journal of the Royal Meteorological Society* **17**, 117-135 (1997).

10 Camberlin, P., Janicot, S. & Poccard, I. Seasonality and atmospheric dynamics of the teleconnection between African rainfall and tropical sea-surface temperature: Atlantic vs. ENSO. *International Journal of Climatology: A Journal of the Royal Meteorological Society* **21**, 973-1005 (2001).

11 Anyamba, A., Tucker, C. J. & Mahoney, R. From El Niño to La Niña: Vegetation response patterns over east and southern Africa during the 1997–2000 period. *Journal of climate* **15**, 3096-3103 (2002).

12 Philippon, N., Martiny, N., Camberlin, P., Hoffman, M. & Gond, V. Timing and patterns of the ENSO signal in Africa over the last 30 years: Insights from normalized difference vegetation index data. *Journal of Climate* **27**, 2509-2532 (2014).

13 Anyamba, A., Glennie, E. & Small, J. Teleconnections and interannual transitions as observed in African Vegetation: 2015–2017. *Remote Sensing* **10**, 1038 (2018).

14 Philippon, N., Martiny, N. & Camberlin, P. Forecasting the vegetation photosynthetic activity over the Sahel: a model output statistics approach. *International Journal of Climatology: A Journal of the Royal Meteorological Society* **29**, 1463-1477 (2009).

15 Frauen, C., Dommenget, D., Tyrrell, N., Rezny, M. & Wales, S. Analysis of the nonlinearity of El Niño–Southern Oscillation teleconnections. *Journal of Climate* **27**, 6225-6244 (2014).

16 Wenhaji Ndomeni, C., Cattani, E., Merino, A. & Levizzani, V. An observational study of the variability of East African rainfall with respect to sea surface temperature and soil moisture. *Quarterly Journal of the Royal Meteorological Society* **144**, 384-404 (2018).

17 Wolff, C. *et al.* Reduced interannual rainfall variability in East Africa during the last ice age. *Science* **333**, 743-747 (2011).

18 Yang, Y., Fang, J., Ma, W. & Wang, W. Relationship between variability in aboveground net primary production and precipitation in global grasslands. *Geophysical Research Letters* **35** (2008).

19 Xie, S.-P. *et al.* Indian Ocean capacitor effect on Indo–western Pacific climate during the summer following El Niño. *Journal of Climate* **22**, 730-747 (2009).

20 Cai, W. *et al.* Pantropical climate interactions. *Science* **363** (2019).

21 Liu, W., Cook, K. H. & Vizy, E. K. Influence of Indian Ocean SST regionality on the East African short rains. *Climate Dynamics* **54**, 4991-5011 (2020).

22 Latif, M., Dommenget, D., Dima, M. & Grötzner, A. The role of Indian Ocean sea surface temperature in forcing East African rainfall anomalies during December–January 1997/98. *Journal of Climate* **12**, 3497-3504 (1999).
23 Stuecker, M. F., Timmermann, A., Jin, F.-F., McGregor, S. & Ren, H.-L. A combination mode of the annual cycle and the El Niño/Southern Oscillation. *Nature Geoscience* **6**, 540-544 (2013).
24 Ryan, K. C. Vegetation and wildland fire: implications of global climate change. *Environment International* **17**, 169-178 (1991).
25 Chikamoto, Y., Timmermann, A., Stevenson, S., DiNezio, P. & Langford, S. Decadal predictability of soil water, vegetation, and wildfire frequency over North America. *Climate Dynamics* **45**, 2213-2235 (2015).
26 Archibald, S., Roy, D. P., van Wilgen, B. W. & Scholes, R. J. What limits fire? An examination of drivers of burnt area in Southern Africa. *Global Change Biology* **15**, 613-630 (2009).
27 Westerling, A. L., Gershunov, A., Brown, T. J., Cayan, D. R. & Dettinger, M. D. Climate and wildfire in the western United States. *Bulletin of the American Meteorological Society* **84**, 595-604 (2003).
28 De Keersmaecker, W. *et al.* A model quantifying global vegetation resistance and resilience to short-term climate anomalies and their relationship with vegetation cover. *Global Ecology and Biogeography* **24**, 539-548 (2015).
29 Di Lorenzo, E. & Ohman, M. D. A double-integration hypothesis to explain ocean ecosystem response to climate forcing. *Proceedings of the National Academy of Sciences* **110**, 2496-2499 (2013).
30 Preethi, B., Sabin, T., Adedoyin, J. & Ashok, K. Impacts of the ENSO Modoki and other tropical Indo-Pacific climate-drivers on African rainfall. *Scientific reports* **5**, 16653 (2015).
31 Williams, C. & Hanan, N. ENSO and IOD teleconnections for African ecosystems: evidence of destructive interference between climate oscillations. *Biogeosciences* **8**, 27 (2011).
32 Zheng, X.-T., Xie, S.-P. & Liu, Q. Response of the Indian Ocean basin mode and its capacitor effect to global warming. *Journal of climate* **24**, 6146-6164 (2011).
33 Chu, J.-E. *et al.* Future change of the Indian Ocean basin-wide and dipole modes in the CMIP5. *Climate dynamics* **43**, 535-551 (2014).
34 Tao, W. *et al.* Interdecadal modulation of ENSO teleconnections to the Indian Ocean Basin Mode and their relationship under global warming in CMIP5 models. *International Journal of Climatology* **35**, 391-407 (2015).
35 Schneider, U. *et al.* GPCC's new land surface precipitation climatology based on quality-controlled in situ data and its role in quantifying the global water cycle. *Theoretical and Applied Climatology* **115**, 15-40 (2014).
36 Malardel, S. *et al.* A new grid for the IFS. *ECMWF Newsletter* **146**, 23-28 (2016).
37 Rayner, N. *et al.* Global analyses of sea surface temperature, sea ice, and night marine air temperature since the late nineteenth century. *Journal of Geophysical Research: Atmospheres* **108** (2003).
38 Zhu, Z. *et al.* Global data sets of vegetation leaf area index (LAI) 3g and fraction of photosynthetically active radiation (FPAR) 3g derived from global inventory modeling and mapping studies (GIMMS) normalized difference vegetation index (NDVI3g) for the period 1981 to 2011. *Remote sensing* **5**, 927-948 (2013).
39 Randerson, J., Van der Werf, G., Giglio, L., Collatz, G. & Kasibhatla, P. Global Fire Emissions Database, Version 4.1 (GFEDv4). *ORNL DAAC* (2015).
40 Neale, R. B. *et al.* The mean climate of the Community Atmosphere Model (CAM4) in forced SST and fully coupled experiments. *Journal of Climate* **26**, 5150-5168 (2013).
41 Oleson, K. W., Bonan, G. B., Feddema, J., Vertenstein, M. & Kluzek, E. Technical description of an urban parameterization for the Community Land Model (CLMU). *NCAR, Boulder* (2010).
42 Lawrence, D. M. *et al.* Parameterization improvements and functional and structural advances in version 4 of the Community Land Model. *Journal of Advances in Modeling Earth Systems* **3** (2011).
43 Stuecker, M. F., Jin, F.-F., Timmermann, A. & McGregor, S. Combination mode dynamics of the anomalous northwest Pacific anticyclone. *Journal of Climate* **28**, 1093-1111 (2015).

340

Figures

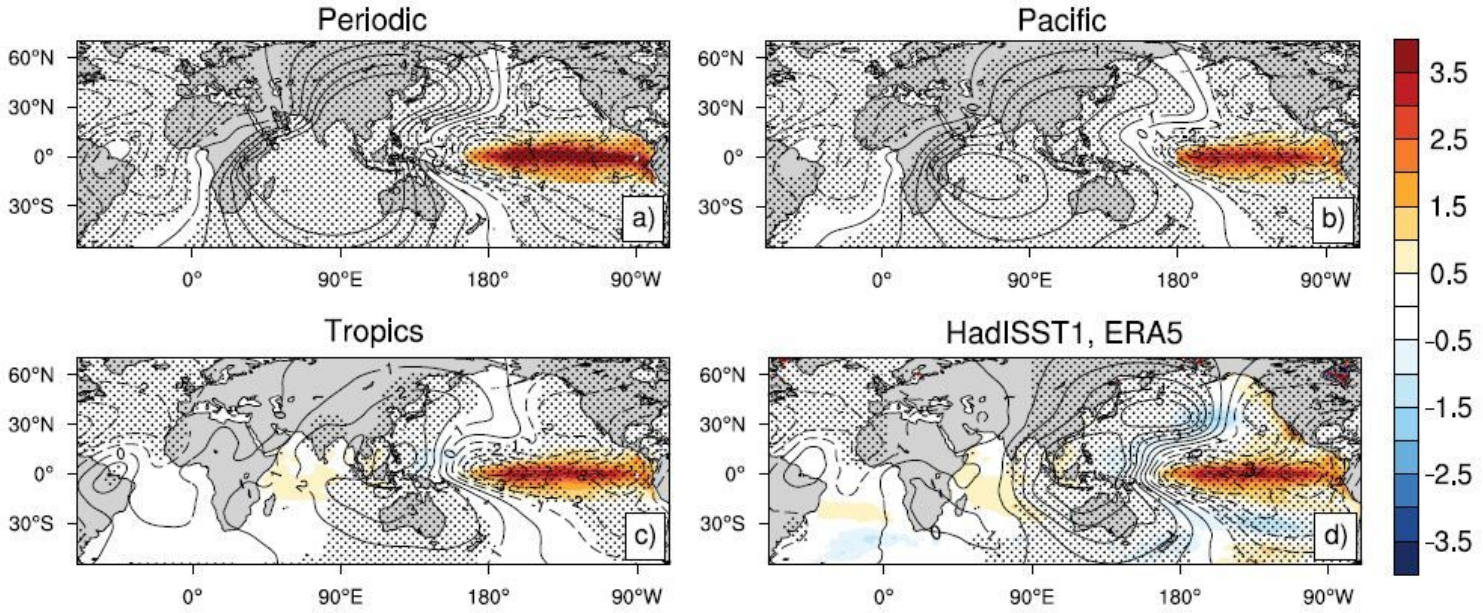

Figure 1

The Periodic and the Pacific experiments (SST anomalies are only prescribed in the tropical Pacific) show pronounced Walker circulation changes between El Niño and La Niña events with anomalous ascending motion over the eastern Pacific region (and corresponding upper-level divergence) and anomalous descending motion (and corresponding upper-level convergence) during the peak ENSO phase of December-January-February [D(0)JF(1)]

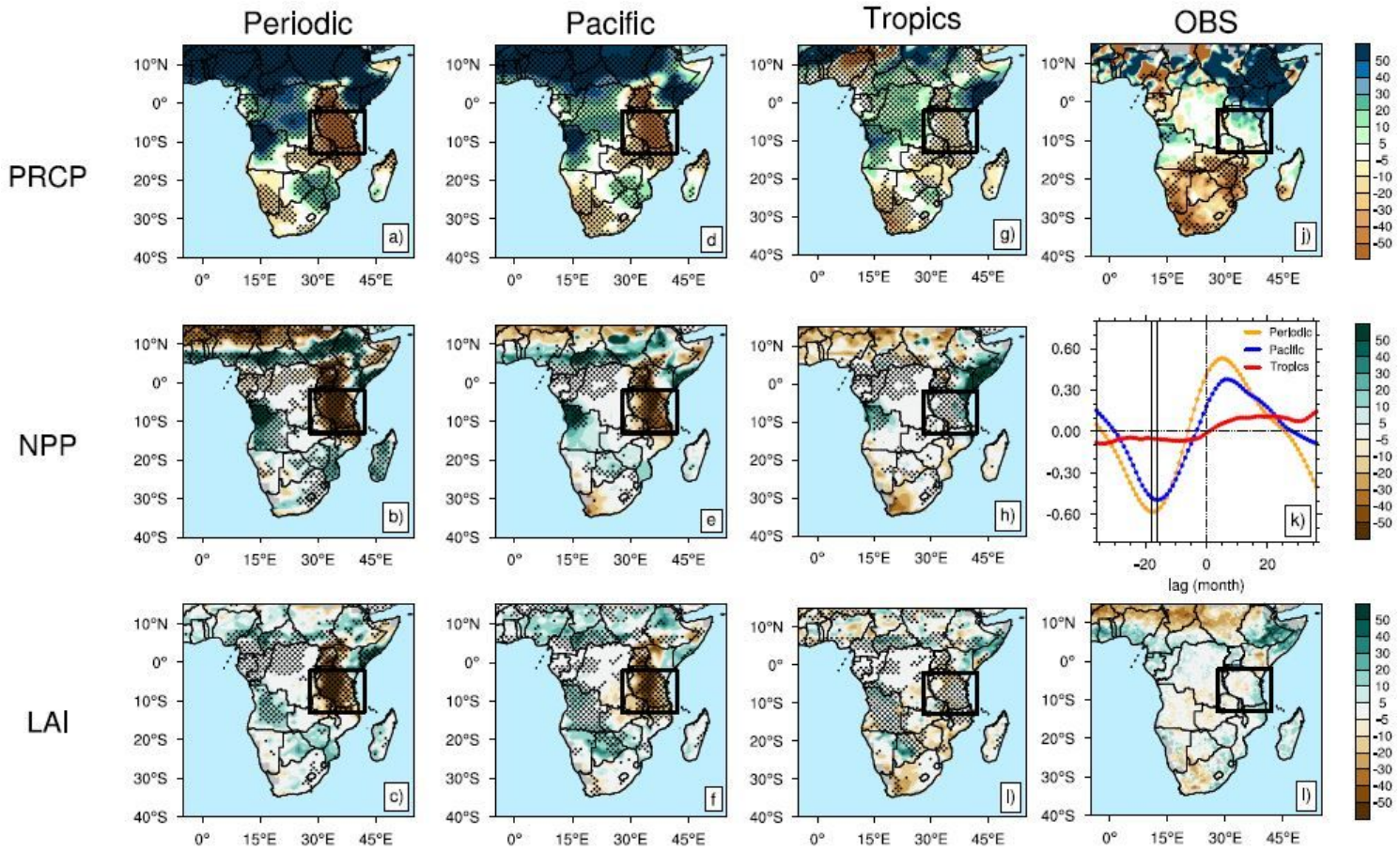

Figure 2

Observed composite differences between El Niño and La Niña events display pronounced positive precipitation anomalies over the Horn of Africa and negative anomalies over Southern Africa in D(0)JF(1)

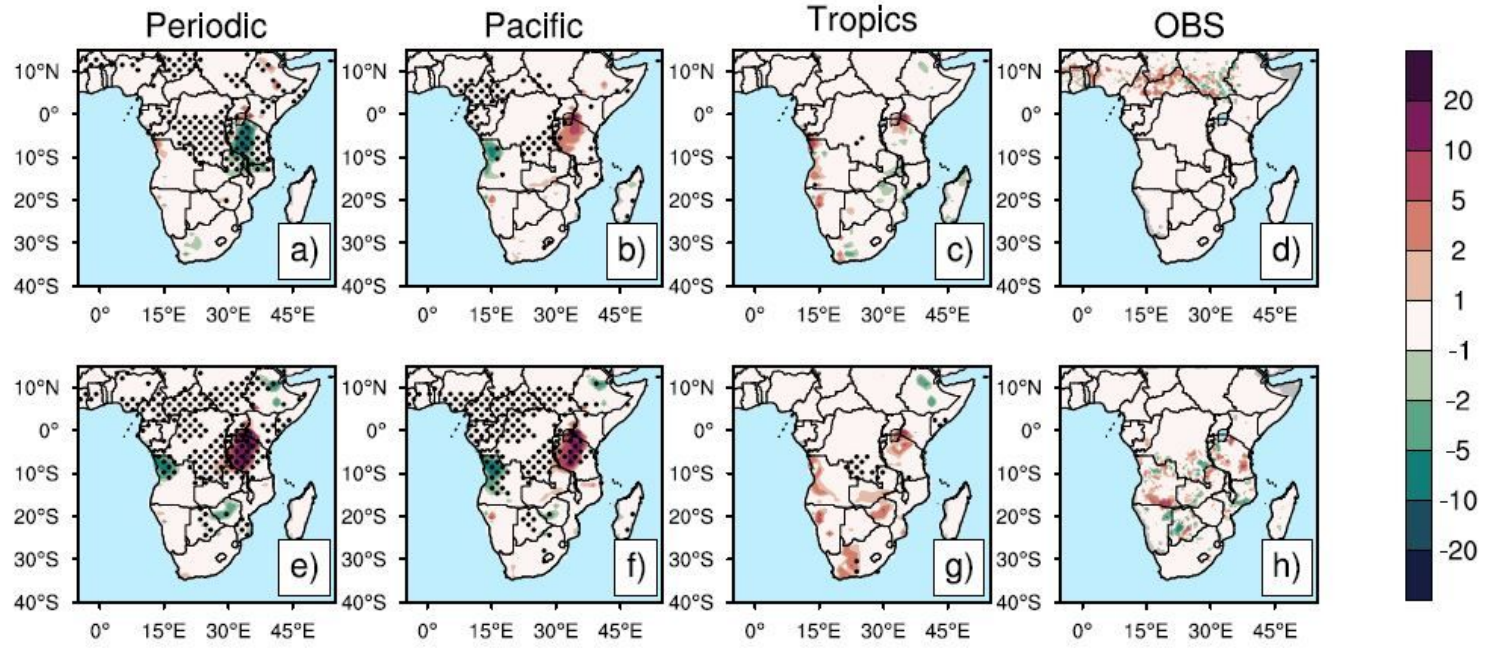

Figure 3

The periodic experiment shows negative anomalies in burned area over Tanzania in D(0)JF(1) and statistically insignificant differences in the Pacific and Tropics experiments, as well as in the observations. However, the Periodic and the Pacific experiments show a 10-20 % increase in burned area over Tanzania in September-October-November in year 1 after ENSO event peak time [SON(1)]

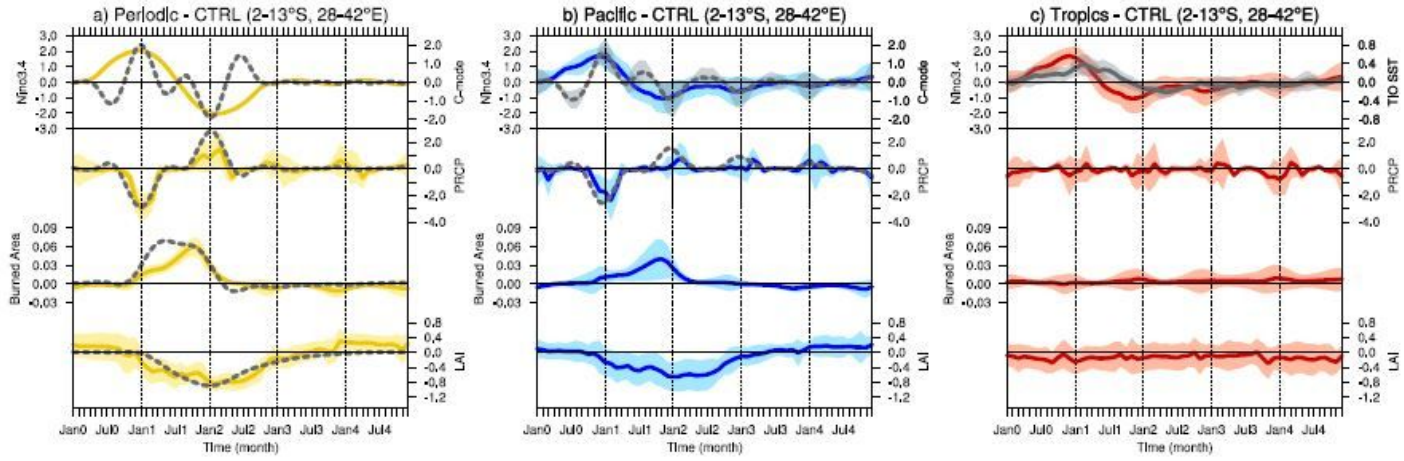

Figure 4

The temporal evolution of the rainfall response over Tanzania to ENSO shows a rapid transition during the peak phase of both El Niño and La Niña in both the Periodic and the Pacific experiments, but not in the Tropics experiment (Fig. 4).

Supplementary Files

This is a list of supplementary files associated with this preprint. Click to download.

- SupportingInformation.docx